

Investigation of phase change characteristics for refrigerant R-134a flow in a double pipe heat exchanger with the use of thermal non-equilibrium model

Mohammed A. Nima* and Raed G. Saihood

Department of Mechanical Engineering, University of Baghdad, 10071 Baghdad, Iraq

Received: 22-October-2022; Revised: 26-May-2023; Accepted: 28-May-2023

©2023 Mohammed A. Nima and Raed G. Saihood. This is an open access article distributed under the Creative Commons Attribution (CC BY) License, which permits unrestricted use, distribution, and reproduction in any medium, provided the original work is properly cited.

Abstract

Almost all thermal systems utilize some type of heat exchanger. In a lot of cases, evaporators are important for systems like organic Rankine cycle systems. Evaporators give a share in a large portion of the capital cost, and their cost is significantly attached to their size or transfer area. Open-cell metal foams with high porosity are taken into consideration to enhance thermal performance without increase the size of heat exchangers. Numerous researchers have tried to find a representation of the temperature distribution closer to reality due to the different properties between the liquid and solid phases. Evaporation heat transfer in an annular pipe of double pipe heat exchanger (DPHEX) filled with copper foam is investigated numerically with utilizing the local thermal non-equilibrium (LTNE) model. Warm water with constant inlet conditions flows in the inner pipe while R143a is used as cooling fluid in the annular pipe. The effects of pores per inch (PPI), mass flux of R134a and copper foam porosity on solid and fluid temperatures, liquid saturation and heat transfer coefficient are analysed and illustrated. Forchheimer-extended Darcy flow model is utilized with the adopting of the two-phase mixture model (TPMM). The governing equations in two-dimensional steady state regime were written in LTNE model. These equations were discretized using the finite volume method and a MATLAB program was built to solve these equations with its initial and boundary conditions. The obtained data illustrates that LTNE effect in metal foam is important for lower porosity, lower pore density and higher mass flux. The ratio of liquid will arrive its lowest value at the outlet, and it decreases with PPI increase and it increases with porosity and mass flux increase. The mean heat transfer coefficient approximately doubled when PPI increased from 10 to 50 and it increased by 70% when porosity decreased from 0.95 to 0.85.

Keywords

Metal foam, TPMM, Flow boiling, LTE and LTNE models, R134a.

1. Introduction

As a result of the wide applications of heat exchangers in various industries, enhancing their efficiency has always been vital in the thermal design of various engineering systems. Therefore, many researchers work to improve the efficiency of this type of heat exchangers. These improvements can be obtained by adding obstacles to the flow to give a longer time for the heat exchange process or by increasing the surface area of heat exchange between the fluid and the warm surface (adding fins or porous media).

Metal foams, as a developed type of porous media, are brilliant applicants for transferring a huge amount of heat with low volumes and production cost.

The most applications of porous materials in energy engineering include solar collectors, fuel cells, regenerators, heat exchangers and heat sinks. The advantages of utilizing metal foams include strong flow-mixing capability in addition to low density and high specific surface area and thermal conductivity. Therefore, many researchers studied the thermal performance of these materials in the past two decades.

Also, evaporation processes within metal foam happen in a wide range of energy applications. Complete evaporation processes within metal foam could be theoretically designated by two models, the separate flow model (SFM) and the two-phase mixture model (TPMM). So, as to eliminate the difficulties related with SFM [1] many modifications of TPMM were presented [2–9], where the sever phases are treated as the elements of two mixtures

*Author for correspondence

and it could be solved on a fixed grid, without need to an intuition information of the phase boundaries, that might be unequal in dimension in addition to transmit in time.

Conferring to the homogenization tactic, two models might be utilized in so far like the temperature field is involved. The local thermal equilibrium (LTE) model is supposed that the temperature of solid and fluid phases is equal at each point. While local thermal non-equilibrium (LTNE) model is assumed that the temperature of solid and fluid phases is locally different. Thus, energy equation is solved separately for each phase whereas one energy equation may be utilized for both phases. These two models may be used to emulate the evaporation process through porous media, though all basic variables of TPMM [2] depend on the supposition of LTE model. In last decades, considerable interest had been rewarded to LTNE model because it is very accurate for simulate the local temperature of solid and fluid phases [3–9].

Mainly in the evaporation area, where the fluid temperature stills fixed according to the thermodynamic theories, the energy transfer from the warm surface is controlled by conduction with the metal foam. The temperature of fluid and solid phases in this area are different, though this difference cannot be considerable, then the heat transfer coefficient might be awfully high according to low pore size [6]. In this state, LTNE model became more suitable, and it would be meaningful to compare the results obtained from these two models for full evaporation process inside a porous media.

There are many studies on evaporation process through metal-foam filled different channels. Considering its priceless results, it is important to extend these works to better representation of evaporation process through a double pipe heat exchanger (DPHEX). According to the previous literature, all articles were simulated the heating source as a constant heat flux or constant wall temperature. The present article is focused on the modified analysis to the evaporation process of R134a through a porous anulus of a DPHEX with warm water flowing in inner pipe as a heating source. According to the previous literature, this analysis with LTNE model is more accurate than the LTE model for solving the evaporation process with metal foam. The effect of pores per inch (PPI), mass flux and porosity on temperature distribution through the anulus (fluid and metal foam temperatures) and heat

transfer coefficient is investigated in the present article.

The rest of the paper is organized as follows. Literature review was discussed in section 2. Section 3 covers the method. Results and discussion were investigated in section 4. Conclusion is in section 5.

2.Literature review

All the industry processes are simulated to a small prototype then it is constructed and subjected to the identical work conditions. This process is very expensive, and it needs long time to reach to the optimum design. The Computational Fluid Dynamics (CFD) or the commercial programming introduce the numerical analysis to do this role instead of the prototype. CFD is an important technique to simulate the problems, such as heat transfer and fluid flow [10].

Many researchers studied the heat transfer process with metal foam. Chen et al. [11] established numerically the optimum conditions for the use of DPHEX filled with metal foam using the Brinkman-Forchheimer-extended Darcy model (BFDM) and LTE model. They found that heat transfer performance enhanced more with lower Darcy number (Da). Then in designing a heat exchanger filled with metal foam, performance factor was evaluated to matching between pressure drop and heat transfer enhancement. Also, Hamzah and Nima [12] studied the effect of adding ten metal foam obstacles on the thermal characteristics in DPHEX. They used the Darcy and Brinkman- Forchheimer model to simulate the flow in porous regions. They found that the coefficient of heat transfer enhanced by 129 % with adding the metal foam fins in DPHEX. Mohammadi et al. [13] used artificial neural network to optimize the properties of porous baffles such as porosity, permeability and cut ratio for maximum heat transfer and minimum pressure drop in shell and tube heat exchanger. They found that baffle cut has the largest contribution in heat transfer and pressure drop by 88% and 71%, respectively. While permeability contribution was 24% in heat transfer and 7% in pressure drop.

Some investigators examined metal foams inserts that are located regularly. Many experimental works proved that the heat transfer enhanced with the using of metal foam blocks but at the same time the pressure drop also increased. This was proved by Nima and Hajeej [14] when they investigated the thermal performance of DPHEX with blocks of metal

foam. They found that the enhancement in Nusselt number is larger than 80% for all the studied cases. Saleh and Rashid [15] used many techniques to enhance the thermal performance of air solar collector under climate condition of Baghdad city. Their experimental and numerical results showed that the collector with porous media has higher efficiency (56%) compared to wire mesh (52%), Corrugated (34%), finned (30%) and smooth flat plate (26%). A CFD simulations was done by Arjun and Annamalai [16] for analysis evaporation process of horizontal tube covered with metal foam. The diameter of this tube was 25.4 mm at 64.6°C. They optimized the characteristics of metal foam to reach optimum heat transfer rate at Re of 650. They utilized LTE model with continuity and momentum equations to simulate the evaporation process and these equations were solved by Volume of Fluid model. They found that metal foam with 0.8 porosity was the optimum case when it rises the heat transfer rate by 250% compared with pure tube case. Metal foam permeability with the range of 10^{-9} – 10^{-7} increasing always improved the heat transfer coefficient. While foam thickness had a slight effect on heat transfer rate and it was about 1.25mm. Stepanov et al. [17] introduced a simplified analytical form makes a solution convenient for temperature distribution on this type of heat exchanger. They found the heat transfer strength with metal foam is higher at highest porosity ($\varepsilon = 0.6169$) compared to other porous inserts with lower porosity. And their laboratory research proved the ability of constructing new heat exchangers with metal foam that can be used in heat supply systems.

The above research hypothesized that the metal foam and the fluid are in thermal equilibrium, but in fact, there is a difference in temperature between them. Other researchers solved two separate energy equations to obtain a temperature distribution closer to real case. Dehghan et al. [18] analysed numerically the forced convection through entrance region of a porous pipe used Brinkman-Forchheimer-extended Darcy (BFED) equation and LTNE model. They found that the LTNE intensity depends on the porosity, PPI, and the thermal conductivity of fluid to solid phases, and it decreases with increase in porosity and conductivity ratio. Same method was adopted by Xu et al. [19] to investigate the thermal effectiveness for DPHEX with metal foam. They showed numerically that the LTNE model must be used on a heat exchanger fully filled with metal foam when thermal conductivity of solid phase 1000 times that of fluid phase. Also, porosity must be lower than 0.9 and PPI larger than 10 for higher effectiveness.

Also, Trilok et al. [20] done that to analyse the thermal flow characteristics through a channel with variable PPI and porosity. Their results appeared that the porosity and PPI has a considerable effect on heat transfer characteristic in mixed and forced convection, but this effect is very small in natural convection.

While Paknahad et al. [21] developed a new method to solve the conjugate between heat transfer and fluid flow in high porosity metal foam. They used multi-relaxation-time model and regularized lattice Boltzmann model for flow and heat transfer respectively. Their results showed the metal foams temperature drops quickly at high Reynolds number, but the liquid temperature rises slightly. Also, heat transfer coefficient increased by 190% with increase in PPI from 10 to 30 and it decreased by 17.5% porosity decrease from 0.90 to 0.80. Diganjit et al. [22] studied numerically a rectangular solar air heater with single-pass with discrete copper metal foam used LTNE model. The channel was considered a two-dimensional flow with mass flow rates (0.03 to 0.05 kg/s) at constant heat flux of 850 W/m². They investigated three different PPI and porosity of copper foam (10, 0.8769), (20, 0.8567), and (30, 0.92) with three different discrete thicknesses at equal distances at 22 mm, 44 mm, and 88 mm. The Nusselt number was 157.64%, 183.31%, and 218.60% for 22 mm, 44 mm, and 88 mm thicknesses, respectively, higher than the free channel. The thermal performance for 22 mm was 5.02% and 16.61% greater than for 44 mm and 88 mm, respectively.

Tamkhade et al. [23] introduced a numerical simulation and CFD analysis for counter flow of DPHEX with (10 – 50) PPI metal foam saturated water to evaluate its thermal performance. The Ansys fluent modelling utilized k-omega viscous model in flow. This 1.5 m heat exchanger was considered with 9.5 mm stainless steel inner pipe and 28 mm galvanized iron outer pipe. Hot water at 80 oC flowed with 2 lpm through inner tube while annular space with 0.9 porosity metal foam discharged 10 lpm cold water at 30 oC. They found that increase in PPI raise the heat transfer rate and pressure drop for both numerical and mathematical results. Iranmanesh and Moshizi [24] utilized a metal foam layer at inner and outer walls of a horizontal annulus for fully developed forced convection to construct two foam regions and one open region between them. The annulus surfaces were subjected to an asymmetric heating. Governing equations such momentum, continuity, and energy equations with boundary

conditions solved numerically with MATLAB program after simplified them to ordinary differential equations. They investigated the effect of Re , Ra , ε , PPI, and thermal conductivity ratio on thermohydraulic characteristics of the flow. Their results showed that the thermal performance effected significantly with fluid-solid thermal conductivity ratio and it decreases for all partially filled cases compared with empty case at thermal conductivity ratio below of 0.01. While at fully filled case, the critical thermal conductivity ratio raised to 0.006.

Other researchers tried to modified the metal foam properties by coating it or adding some materials to its structure. Maiorano et al. [25] fabricated an aluminum/graphite composite foam by the replication method which infiltrates liquid aluminum with SiC-coated oriented graphite flakes and NaCl particles. Their results showed that foams with large sizes of NaCl have low pressure drops. They found that large graphite flakes coated with SiC gives thermal conductivity 6 times higher and heat dissipation 5 times higher than standard aluminum foams, making them the perfect tool in cooling electronic devices. Ginting et al. [26] modified stainless steel metal foams into superhydrophilic and superhydrophobic surfaces. The superhydrophilic type was used as a wick in a ferrofluid cylindrical heat pipe because of its high wettability and capillary. The cylindrical heat pipe was tested at two heat input variations of 3 and 5 W in a horizontal direction. The thermal performance of this heat pipe gives the maximum thermal resistance of 2.47 °C/W at 5W as a heat input. Optimization of metal foam pellet shapes was studied by George et al. [27] to improve radial heat transfer using a modified version of particle-resolved CFD. Many configurations like external grooves, varied aspect ratios, pellet with inner holes, and as well as various foam morphologies are considered to maximize the pellet geometry. They found that foam ring with the of 2.5 aspect ratio, 0.45 mm cell size, and 0.82 porosity was an optimal case at Re range from 250 to 2250.

Same thing was adopted with studying the evaporation process in metal foam. Some researchers studied the problem under LTE model, and another some investigated it with LTNE model. While other researchers observed new methods for reach to more accurate results with less effort. Wang [2] used LTE assumption with asymmetric discrete heating on a channel. Their results showed that superheated vapor has been created clearly near to the warm surface. At the same time, within a very short distance, a large

change in temperature was observed in the range of 100 °C and 500 °C for steel and glass beads, respectively. The cut-outs in the effective diffusion term may be the reason for these results, or because of utilizing the simplified LTE model. To skip these reasons, a complete evaporation process of water, like that investigated by Wang [2], was numerically simulated by Wang [3] with smoothing the effective diffusion term for these two models. They found that LTE model is unrealistic to estimate the multi-dimensional evaporation problems. Lu and Zhao [4] investigated refrigerant R134a evaporation process in 26 mm horizontal tube filled with metal-foam used TPMM with LTNE model. The study was done for two types of metal foam 20 and 40 PPI with 0.9 porosity. The mass flux was (26 to 106 kg/m².s) with vapor quality up to 0.9. Their results showed that the heat transfer coefficient increases with porosity, PPI, mass flux, and heat flux. And it adopted different trends for low and high mass fluxes as the vapor quality rises.

Alomar et al. [5] presented a new algorithm that rejects the cut-outs in the effective diffusion term through the borders which separates the single to two-phase areas. This algorithm was effectively utilized to analyse the one-dimensional full evaporation process in a divergent porous pipe. Their results showed clearly that inlet conditions and the shape of divergent porous pipe most affect the properties of outlet steam compared to porous media characteristics which have small influence. Then, it was advisable to test the effectiveness of this algorithm for two- or three-dimensional studies with both LTE and LTNE model. A comparison study between LTE and LTNE model is investigated by Xu et al. [6] for a two-dimension fluid flow in a tube filled with metal foam with uniform wall temperature. The SIMPLER algorithm was utilized to solve the conservation equations of mass and momentum in metal foams with correction equation for velocity and it was written as a FORTRAN code. LTNE effect representation was illustrated by solid-fluid temperature difference and relative deviation. Their results showed that the relative deviation was more effective to represent LTNE effect in metal foam. The LTNE effort in metal foam was noticeable for small duct size, low porosity, large ratio for solid to fluid thermal conductivity, low Re , and low PPI. The thermal results showed LTE model is always higher than LTNE model and LTE model is suitable to use metal foams porosity greater than 0.95 or thermal conductivity ratio higher than 0.148 with relative deviation less than 0.2.

This new mathematical model, which depended on the formula of the modified enthalpy of TPMM with LTNE model, was modified by Alomar [7, 8] to represent the full phase change process in porous evaporator with asymmetrical heating. The complete steady two-dimensional evaporation process in a horizontal evaporator filled with porous media was investigated by Alomar [7]. Their results showed that the transition to two-phase zone is more rapidly in the axial direction compared to that in the transverse direction. They illustrated clearly that the utilizing this modified formula is very necessary for simulation the complete evaporation process especially with high heat and mass fluxes. Alomar [8] used this modified formula for the same case with transient condition. They showed that non-Darcian influence leads to clear growth in vapor region in the downward of the channel.

He et al. [1] studied numerically the transient behaviour of phase change process in porous two-phase flow used SPM with LTNE model. With the increase of the heat capacity and the porous media density, the system takes longer to reach a steady state, and the transient degradation of heat transfer and vapor quality effect in the beginning stage are more acute. Liu et al. [9] proposed a new transient mathematical model used TPMM with modified mixture enthalpy and enthalpy ratio to study phase-change transpiration cooling with pressure injection. They found that the variable velocity of mass flow and the volume of heat flux have significant effect on the injection pressure fluctuation, the increase in mass flow and heat flux increases more the variation of injection pressure.

Many experimental studies were investigated evaporation process through metal foam. Flow boiling of R134a in nine mini-channels evaporator with metal foam investigated experimentally by Gao et al. [28] to enhance the performance of electronics cooling. They found that the heat transfer coefficient increases by 150% and it has an opposite trend to that in empty mini-channel. While, the pressure drop increased by 270% and frictional loss represents over 70% of it. Heat transfer coefficient increased significantly with surface heat flux and R134a quality, whereas mass flux had little effect on it. Nam et al. [29] studied experimentally the boiling Heat transfer of R245fa in a vertical rectangular channel filled with various metal foam insert. At the inlet, the vapor ratio was between 0.05 and 0.99 and the mass flux was from 133 to 300 kg/m²s with constant saturation pressure at 5.9 bar. High-speed

visualization experiment was used to visualize the two-phase flow phenomena. The boiling heat transfer coefficient with metal foam inserts had the same behaviour as that of the fully filled channel but it dropped quickly when the vapor ratio was close to 1. While the pressure drop decreased by 1/8 times compared with that of the fully filled channel. Thermal performance of evaporation heat transfer of the copper foam wicks was investigated experimentally for heat pipes by Li et al. [30]. The magnetron sputtering was utilized to construct this type of metal foam wicks by mix the copper foam with zinc oxide (ZnO) nanoparticles. They tested the effect of capillary performance, contact angle, and microscopic appearance on thermal performance of heat pipe. Their results show that thermal performance was enhanced with low PPI copper foams 30 or 70 PPI while the 110 PPI copper foam had an opposite effect. They found that thermal performance enhanced strongly for 30 PPI and the evaporation heat transfer coefficient increased by 29.35% and 80.14%, compared with 70 and 110 PPI respectively after 12 hours of magnetron sputtering. Recently, hydrothermal properties of flow boiling for R134a annular tubes filled with copper-foam were investigated experimentally by Nosrati et al. [31]. The 30 cm test tube, with 14.3 mm and 4.7 mm outer and inner diameters, is filled with 10 and 20 PPI copper foam. The mass flux was 10 to 80 kg/m².s with vapor quality of 0.13-0.85. The test section was heated with constant uniform heat flux of 5.7 kW/m². They found that the heat transfer coefficient is improved by 220% with utilizing 20 PPI. Kisitu et al. [32] tested the effect of compressed and uncompressed copper foam on heat transfer and fluid flow characteristics off R134a evaporators. The tests were conducted for copper foam (25.4 × 25.4 × 2.5 mm) with 40 PPI and porosities of 0.62–0.91. The test section subjected to uniform heat flux of 7 - 174 W/cm² and mass flux was 150 - 375 kg/m²s at saturation temperatures of 31 to 33 °C. They compared compressed metal foam (compressing the foam by up to 4X) with and they found that the compressed metal foam had three-times lower thermal resistance and enhanced critical heat transfer. The heat transfer coefficient in compressed metal foam increased the vapor quality about 75%, and the pressure drop increased linearly with increase in vapor quality at the exit.

Water boiling in multi-walled nanotube coating on a copper foam was studied by Kang et al. [33]. Their results showed that this type of copper foam increased the critical heat flux by 340% and the heat

transfer coefficient by 250% compared to a polished Cu surface. Then the performance of pool boiling enhanced with utilizing this type of metal foam. They used a high-speed camera to illustrate the bubble growth during the boiling process and same results were returned from ANSYS Workbench simulation. Lattice Boltzmann method was used by Li et al. [34] to study the effect of surface roughness and pulse heating to achieve higher heat transfer efficiency. Their results showed that the boiling regions of pulse heating are greater compared with constant heating and boiling rate increase as pulse amplitude increase. Under When critical temperature larger than 1.09 of boiling temperature, the heat transfer coefficient with pulse heating raised by 30.54% compared with that at constant heating, and it decreases with the increase of vapor.

Laterally, many researchers studied the effect of gradient arrangement of metal foam on the boiling heat transfer performance. Yue et al. [35] studied numerically nonuniform temperature distribution through horizontal gradient porous metals. They utilized lattice Boltzmann model to solve the problem of pool boiling heat transfer performances of horizontal gradient porous metals are studied by phase-change. Their results showed that gradient metal foam could be achieve a real separation between liquid and vapor phases, make the bubble collapse freely, enhance the preparing of fresh liquid, and increase the boiling performance. This configuration of metal foam with higher thermal conductivity or lateral hydrophobic surface promoted a uniform temperature distribution through the heating surface at low heat flux. They provided a novel solution to enhance the chip wall temperature homogeneity for the steady work of electronic equipment. While, boiling of deionized water heat transfer was studied experimentally by Wang et al. [36] through (100 × 100 × 250) mm copper foam bilayers which arranged in positive (PPI decreases towards top side) or inverse gradients. Their results showed that the heat transfer increases by 60% for gradient type compared with a uniform. For the positive gradient arrangement, thermal performance first raised with PPI, then lowered with PPI increase above of 60 PPI. While for inverse gradient, thermal performance was affected sparingly with PPI increase. According to the literature review, many researchers tried to specify a suitable mathematical model to get a more realistic representation of

thermohydraulic properties for evaporation process with metal foam. Most previous articles studied the problem with boundary condition as constant temperature or heat flux on the wall. In this article DPHEX has been taken into account to so that the problem is closer to the real situation.

3. Methods

3.1 Problem description

The physical model of this paper is a counter-flow, DPHEX of length $L = 2000$ mm, as illustrated in *Figure 1*. The radius of inner and annular pipes is $r_i = 25$ mm and $r_o = 75$ mm, respectively. The hot fluid (water) and cold fluid (R143a) flowing in inner and annular pipes, respectively. The annular pipe of the heat exchanger is filled with copper foam and its outer surface is thermally insulated. The effect of radiation heat transfer and the heat conduction through interface-wall are negligible. For simplification, the exit condition for temperature and velocity are assumed fully developed and the flow is incompressible with constant physical properties.

3.2 Assumptions

The most important presumptions which govern this problem are:

a- Annular pipe

- 1) The metal foam is fully saturated with R134a and it is uniform, rigid and isotropic porous media.
- 2) LTNE model is utilized to represent fluid and solid phases.
- 3) The mixture velocity is determined by utilizing Ergun expression for the model of Forchheimer-extended Darcy flow.
- 4) The fluid in evaporation area is fixed at constant saturation temperature.
- 5) The thermo-physical characteristics of R134a and metal foam are constant.
- 6) The thermal dispersion and diffusion which resulted from the nature of the metal foam are negligible.

B- Inner pipe

- 1) Laminar two- dimensional water flow
- 2) Thermo-physical properties of water are assumed constant except its density which treated according to Boussinesq approximation (in momentum equation).
- 3) Viscous dissipation and internal heat generation are negligible.

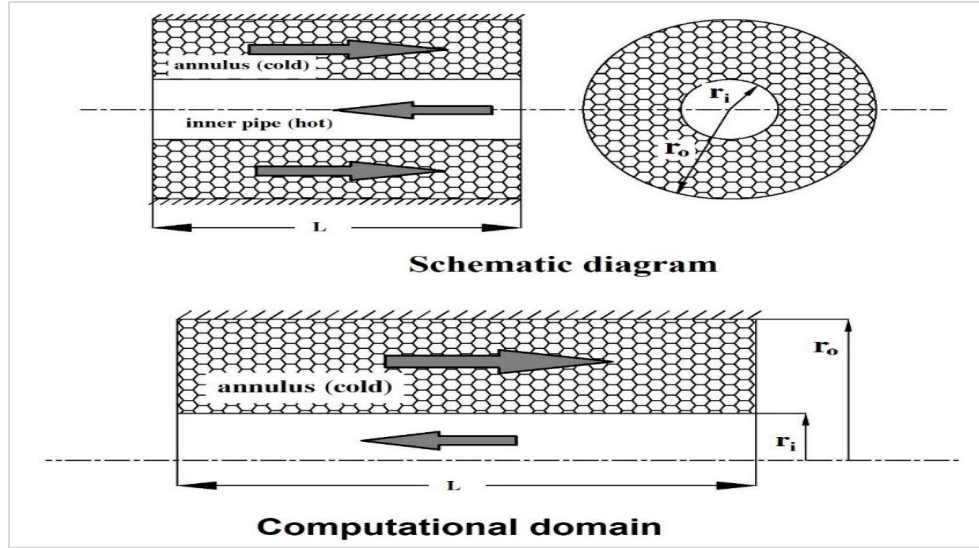


Figure 1 DPHEX filled with metallic foams for counter-flow arrangement

3.3 Governing equations

3.3.1 Annular pipe

Darcy equation is utilized for the flow in porous media with unity or smaller Reynolds number Re_p . The term of velocity square ought to be added in Darcy term to decrease the resulted error for elevated velocities. The flow model of Forchheimer-extended Darcy is shown in Equation (1) [37].

$$\nabla p = -\frac{K}{\mu} \mathbf{u} - \beta \rho |\mathbf{u}| \mathbf{u} \tag{1}$$

Where p , K , ρ , μ , \mathbf{u} represent the pressure, metal foam permeability, density, dynamic viscosity and superficial velocity vector respectively.

β represents the Forchheimer’s coefficient, it can be calculated as follows:

$$\beta = \frac{C_E}{\sqrt{K}} \tag{2}$$

where C_E is Ergun constant.

Substitute Equation 1 into Equation 2, Equation 1) will be:

$$\nabla p = -\frac{K}{\mu} \mathbf{u} - \frac{C_E}{\sqrt{K}} \rho |\mathbf{u}| \mathbf{u} \tag{3}$$

Where (6):

$$K = 0.00073(1 - \varepsilon)^{-0.224} (d_f/d_p)^{-1.11} d_p^2 \tag{4}$$

$$C_E = 0.00212(1 - \varepsilon)^{-0.132} (d_f/d_p)^{-1.63} \tag{5}$$

$$d_p = 0.0254/\omega \tag{6}$$

$$d_f = 1.18d_p \sqrt{(1 - \varepsilon)/3\pi} / [1 - e^{-(1-\varepsilon)/0.04}] \tag{7}$$

$$d = (1 - e^{-(1-\varepsilon)/0.04}) d_f \tag{8}$$

Where, d_p , d_f , d are particle diameter, Reynolds number based on particle diameter is:

$$Re_p = |\mathbf{u}| d / \nu_f \tag{9}$$

According to the above debate and with the ($Re_p > 1$) that taken in this article, TPMM will be used with Forchheimer-extended Darcy flow. The governing equations for R134a as follows:

$$\nabla \cdot (\rho \mathbf{u}) = 0 \tag{10}$$

2) Momentum conservation:

$$\rho \mathbf{u} = -\frac{K}{\nu + C_E \sqrt{K} |\mathbf{u}|} [\nabla p - \rho_k \mathbf{g}] \tag{11}$$

Where ν and \mathbf{g} are the kinetic viscosity and gravitational acceleration vector respectively.

3) Energy conservation for R134a:

$$\Omega \frac{\partial H}{\partial t} \nabla \cdot (\gamma_h \mathbf{u} H) = \nabla \cdot (\Gamma_h \nabla H) + \nabla \cdot \left[f_s \frac{K \Delta \rho h_{fg}}{\nu_v} \mathbf{g} \right] + Q_{sf} \tag{12}$$

Where t , Ω , H , γ_h , Γ_h , f_s , $\Delta \rho$, h_{fg} and Q_{sf} represent the time, effective heat capacitance ratio, volumetric enthalpy, two-phase advection correction coefficient, effective thermal diffusion coefficient, hindrance function, density difference = $(\rho_l - \rho_v)$, heat transfer coefficient between solid-phase and fluid-phase and volumetric heat transfer rate between solid-phase and

fluid-phase respectively, and the subscript l and v refer to liquid and vapor phases.

$$\mathbf{g} = -g\hat{r} \quad (13)$$

Where r is the radial direction

The mixture characteristics in Equations 10 to 12 are written as:

Density:

$$\rho = \rho_l s + \rho_v (1 - s) \quad (14)$$

Velocity:

$$\rho \mathbf{u} = \rho_l \mathbf{u}_l + \rho_v \mathbf{u}_v \quad (15)$$

Mixture enthalpy h and volumetric enthalpy H:

$$\rho h = \rho_l s h_l + \rho_v (1 - s) h_v \quad (16)$$

$$H = \rho (h - 2h_{vsat}) \quad (17)$$

Kinetic density:

$$\rho_k = \rho_l \lambda_l(s) + \rho_v \lambda_v(s) \quad (18)$$

Viscosity:

$$\mu = \frac{\rho_l s + \rho_v (1-s)}{k_{rl}/v_l + k_{rv}/v_v} \quad (19)$$

Where s and λ are the liquid saturation and relative mobility respectively, and the subscript sat refers to saturation state.

$$T = \begin{cases} \frac{H+2\rho_l h_{vsat}}{\rho_l c_l} & H \leq -\rho_l (2h_{vsat} - h_{lsat}) \\ T_{sat} & -\rho_l (2h_{vsat} - h_{lsat}) < H \leq -\rho_v h_{vsat} \\ T_{sat} + \frac{H+\rho_v h_{vsat}}{\rho_v c_v} & -\rho_v h_{vsat} < H \end{cases} \quad (25)$$

$$s = \begin{cases} 1 & H \leq -\rho_l (2h_{vsat} - h_{lsat}) \\ \frac{H+\rho_v h_{vsat}}{\rho_l h_{fg} + (\rho_l - \rho_v) h_{vsat}} & -\rho_l (2h_{vsat} - h_{lsat}) < H \leq -\rho_v h_{vsat} \\ 0 & -\rho_v h_{vsat} < H \end{cases} \quad (26)$$

The velocity of liquid and vapor phases can be determined from the flow model of Forchheimer-extended Darcy, Equation 11, as follows 37:

$$\rho_l \mathbf{u}_l = -\frac{K k_{rl}}{v_l + c_E \sqrt{K k_{rl}} |\mathbf{u}_l|} [\nabla p_l - \rho_l \mathbf{g}] \quad (27)$$

$$\rho_v \mathbf{u}_v = -\frac{K k_{rv}}{v_v + c_E \sqrt{K k_{rv}} |\mathbf{u}_v|} [\nabla p_v - \rho_v \mathbf{g}] \quad (28)$$

where ∇P_l and ∇p_v are defined as:

$$\nabla P_l = \nabla P + \lambda_l(s) \nabla P_c(s) \quad (29)$$

$$\nabla p_v = \nabla p + \lambda_v(s) \nabla p_c(s) \quad (30)$$

The hindrance function can be calculated as follows:

$$f(s) = \frac{k_{rv} k_{rl} / v_l}{k_{rl} / v_l + k_{rv} / v_v} \quad (31)$$

The relative permeabilities k_{rl} and k_{rv} are defined in Equations 32 and 33.

Advection correction coefficient:

$$\gamma_h = \frac{[(\rho_v/\rho_l)(1-s)+s][h_{vsat}(1+\lambda_l)-h_{lsat}\lambda_l]}{(2h_{vsat}-h_{lsat})s+(\rho_v h_{vsat}/\rho_l)(1-s)} \quad (20)$$

Effective heat capacitance ratio:

$$\Omega = \varepsilon + \rho_s c_s (1 - \varepsilon) \frac{dT}{dH} \quad (21)$$

Where ε , c and T represent the porosity, specific heat capacity and temperature respectively, and the subscript s refers to solid phase (metal foam).

Effective thermal diffusion coefficient:

$$\Gamma_h = \frac{1}{1+(1-\rho_v/\rho_l)h_{vsat}/h_{fg}} D(s) + k_{feff} \frac{dT}{dH} \quad (22)$$

Capillary diffusion coefficient:

$$D(s) = \frac{\sqrt{\varepsilon K \sigma}}{\mu_l} \frac{k_{rl} k_{rv}}{(v_v/v_l)k_{rl} + k_{rv}} [-J'(s)] \quad (23)$$

Where k represents the thermal conductivity and the subscript f, r and eff refer to fluid phase, relative and effective respectively.

Relative mobility:

$$\lambda_l(s) = \frac{k_{rl}/v_l}{k_{rl}/v_l + k_{rv}/v_v}, \quad \lambda_v(s) = \frac{k_{rv}/v_v}{k_{rl}/v_l + k_{rv}/v_v} \quad (24)$$

The temperature of R134a and its liquid saturation can be determined as follows:

The following constitutive relations are used to calculate the relative permeabilities and the capillary pressure:

$$k_{rl} = s^3 \quad (32)$$

$$k_{rv} = (1 - s)^3 \quad (33)$$

$$p_c(s) = \sqrt{\frac{\varepsilon}{K}} \sigma J(s) \quad (34)$$

where;

$$J(s) = 1.417(1 - s) - 2.12(1 - s)^2 + 1.263(1 - s)^3 \quad (35)$$

The restrictions of utilizing LTNE model assume to add a separate energy equation for the solid phase as:

$$\nabla \cdot (k_{seff} \nabla T_s) - Q_{sf} = 0 \quad (36)$$

The effective thermal conductivity can be calculated as follows (6):

$$k_{eff} = \frac{1}{\sqrt{2}(R_A + R_B + R_C + R_D)} \quad (37)$$

Where;

$$R_A = \frac{4\chi}{(2e^2 + \pi\chi(1-e))k_s + (4 - 2e^2 - \pi\chi(1-e))k_f} \quad (38)$$

$$R_B = \frac{(e - 2\chi)}{e^2 k_s + (2 - e^2)k_f} \quad (39)$$

$$R_C = \frac{(\sqrt{2} - 2e)}{\sqrt{2}\pi\chi^2 k_s + (2 - \sqrt{2}\pi\chi^2)k_f} \quad (40)$$

$$R_D = \frac{2e}{e^2 k_s + (4 - e^2)k_f} \quad (41)$$

$$\chi = \sqrt{\frac{\sqrt{2}(2 - 2e - 3\sqrt{2}/4e^3)}{\pi(3 - 4\sqrt{2}e - e)}} \quad , \quad e = 0.198 \quad (42)$$

$$k_{seff} = k_{eff}|_{k_f=0} \quad , \quad k_{feff} = k_{eff}|_{k_s=0} \quad (43)$$

$$k_f = \varepsilon[k_l s + k_v(1 - s)] \quad (44)$$

Equation 43 represents the actual thermal conductivity for each phase that which is appropriated with the assumption of neglecting the thermal diffusion and dispersion.

According to using LTNE model, some heat will be transferred between the fluid and the solid phases (Q_{sf}). It can be written as:

$$Q_{sf} = h_{sf} a_{sf} (T_s - T_f) \quad (45)$$

where;

a_{sf} , typifies the contacting area of solid-fluid per unit volume as (37):

$$a_{sf} = 3\pi d_f [1 - e^{-(1-\varepsilon)/0.04}] / (0.59 d_p)^2 \quad (46)$$

h_{sf} , typifies the coefficient of heat transfer from solid to fluid as (37):

$$h_{sf} = 0.26 Pr^{0.37} Re_p^{0.6} k_f / d \quad (47)$$

Where Pr is Prandtl number.

According to the pool boiling correlation developed by Rohsenow [38], the boiling heat transfer in the two-phase region ($0 < s < 1$) will be determined as:

$$q_{boil} = \mu_l h_{fg} \left(\frac{g(\rho_l - \rho_v)}{\sigma} \right)^{1/2} \left(\frac{c_l(T_s - T_{sat})}{C_{sf} h_{fg}} \right)^3 Pr^{1.7/0.33} \quad (48)$$

Where σ and C_{sf} relies on the surface tension and the conjunction for the cooling fluid with the warm surface. In this article $C_{sf} = 0.0053$ is taken for (R134a-copper).

Lastly, the solid to fluid heat transfer (Q_{sf}) in the evaporation area may be represented by balancing the evaporation heat in Equation 45 with the saturated liquid:

$$Q_{sf} = a_{sf} s q_{boil} \quad (49)$$

Thermo-physical characteristics of R134a, pure water and copper foam are introduced in *Table 1*.

3.3.2 Inner pipe

The Equation of Navier-Stokes is used to model the flow in the inner pipe, also, the energy equation is used to solve the thermal field. The governing Equations given as;

Conservation of Mass:

$$\frac{\partial \rho_h}{\partial t} + \nabla \cdot (\rho_h \mathbf{u}_h) = 0 \quad (50)$$

Conservation of Momentum:

$$\rho_h \frac{\partial \mathbf{u}_h}{\partial t} + (\mathbf{u}_h \cdot \nabla) \mathbf{u}_h = -\nabla p_h + \mu_h \nabla^2 \mathbf{u}_h + \rho_h \mathbf{g} \quad (51)$$

Conservation of Energy:

$$(\rho C_p)_h \left(\frac{\partial T_h}{\partial t} + (\mathbf{u}_h \cdot \nabla) T_h \right) = k_h \nabla^2 T_h \quad (52)$$

The subscript h refers to hot water.

Table 1 Thermo-physical properties of R134a, water and copper foam

Property	Symbol	Copper	R134a	Water	
		Solid	Liquid	Vapor	Liquid
Density	ρ kg/m ³	8954	1218	29.54	957.9
Thermal conductivity	k^* (W/m K)	386	0.0824	0.01353	0.679
Specific heat	C (J/kg K)	383.1	1413	1013	4217
Dynamic viscosity	μ (kg/m.s)	---	2.055×10^{-4}	1.167×10^{-5}	2.82×10^{-4}
Interfacial tension	σ (N/m)	---	0.00848	---	---
Latent heat of evaporation	h_{fg} (J/kg)	---	180500	---	---

3.4 Initial and boundary conditions

The operation conditions are assumed as:

1) Initial Conditions (at $t = 0$)

For annular pipe:

$$\left. \begin{aligned} u &= v = 0 \\ T_s &= T_f = T_{in} \\ p &= 6 \text{ bar} \\ H &= \rho_l (c_l T_{in} - 2h_{vsat}) \end{aligned} \right\} \quad (53)$$

For inner pipe:

$$\left. \begin{aligned} u_h = v_h = 0 \\ T_h = 40^\circ\text{C} \\ p_h = 0 \end{aligned} \right\} \quad (54)$$

2)Boundary Conditions

For annular pipe:

$$\left. \begin{aligned} \text{At } x = 0, R_i < r < R_o \text{ (inlet)} \\ u = 0, v = v_{in} \\ T_s = T_{in} \\ H = \rho_l(c_l T_{in} - 2h_{vsat}) \\ p = 6 \text{ bar} \end{aligned} \right\} \quad (55)$$

$$\left. \begin{aligned} \text{At } x = L, R_i < r < R_o \text{ (outlet)} \\ \frac{\partial u}{\partial x} = 0 \\ \frac{\partial T_s}{\partial x} = 0 \\ \frac{\partial H}{\partial x} = 0 \\ \frac{\partial p}{\partial x} = 0 \end{aligned} \right\} \quad (56)$$

$$\left. \begin{aligned} \text{At } 0 < x < L, r = R_o \text{ (adiabatic wall)} \\ u = v = 0 \\ (1 - \varepsilon)k_s^* \frac{\partial T_s}{\partial x} = 0 \\ -\Gamma_h \frac{\partial H}{\partial x} + f_s \frac{K \Delta \rho h_{fg}}{v_v} g \sin \phi = 0 \end{aligned} \right\} \quad (57)$$

For inner pipe:

$$\left. \begin{aligned} \text{At } x = L, 0 < r < R_i \text{ (inlet)} \\ u_h = 0, v_h = 0 \\ T_h = 40^\circ\text{C} \end{aligned} \right\} \quad (58)$$

$$\left. \begin{aligned} \text{At } x = 0, 0 < r < R_i \text{ (outlet)} \\ \frac{\partial u_h}{\partial x} = 0, v_h = 0 \\ \frac{\partial T_h}{\partial x} = 0 \\ \frac{\partial p_h}{\partial x} = 0 \end{aligned} \right\} \quad (59)$$

$$\left. \begin{aligned} \text{At } 0 < x < L, r = 0 \text{ (symmetric axis)} \\ \frac{\partial u_h}{\partial r} = 0, v_h = 0 \\ \frac{\partial T_h}{\partial r} = 0 \\ \frac{\partial p_h}{\partial r} = 0 \end{aligned} \right\} \quad (60)$$

For interface wall

$$\left. \begin{aligned} \text{At } 0 < x < L, r = R_i \\ u = v = 0 \\ (1 - \varepsilon)k_s^* \frac{\partial T_s}{\partial x} = q_s \\ \Gamma_h \frac{\partial H}{\partial x} - f_s \frac{K \Delta \rho h_{fg}}{v_v} g = q_f \end{aligned} \right\} \quad (61)$$

where;

$$q_s + q_f = q_w = k_h \frac{\partial T_h}{\partial r} \quad (62)$$

Where x , R_i and R_o are the axial direction, inner and outer dimeters respectively, and the subscript in and w are inlet and wall conditions.

With respect to LTNE model, solid and fluid phases will soak up a different quantity of heat rate (q_s and q_f) from the overall heat transfers from warm water to R134a-copper region (q_w) at $r = R_i$. Xiao et al. [39] developed an equation addition to Equation 62 to divide the total heat transfer (q_w) into q_s and q_f , this achieves the combination between heat conduction in a solid wall and energy transfer in the porous media:

$$\frac{q_f}{q_s} = \frac{k_{f,eff} T_{wf} - T_f}{k_{s,eff} T_{ws} - T_s} \quad (63)$$

where;

T_f and T_s , represent temperatures of R134a and copper foam near the wall of inner pipe.

T_{wf} and T_{ws} , represent temperatures of R134a and copper foam at the wall of inner pipe. Where, q_f will drop to zero in the evaporation area, Equation 63, according to the assumption of the evaporation is an isothermal process in that region.

3.5 Numerical procedure

In this study, the finite volume method is applied to discretize the momentum equation and solved by SIMPLE algorithm of Patanka [40].The velocity field is obtained from this equation after computing the pressure field. Then, Equations 27 and 28 are used to calculate liquid and vapor velocities and its values are stored at the control volumes interfaces.

Based on the conservation of mass equation, the pressure at the exit boundary ($P_{i,jmax}^{k+1}$) is computed as:

$$\frac{P_{i,jmax}^{k+1} - P_{i,jmax-1}^k}{\Delta r} = -G'' \left[\frac{\rho v (v + C_E \sqrt{K} |u|)}{K} \right]_{i,jmax}^k \quad (64)$$

where G'' , is:

$$G'' = \frac{\dot{m}}{\int (\rho v)_{i,jmax} dx} \quad (65)$$

The mass flow rate ratio G'' will approach unity combined with achieving the overall mass conservation then the pressure field will be received on the whole domain.

Then, an implicit control volume formulation is utilizing to solve the energy equation of fluid phase by use the power law scheme of Patankar [40]. Equations 25 and 26 is solved to calculate the temperature and the ratio of liquid from the enthalpy. Finally, the energy equation of solid phase is solved to calculate the temperature of the solid phase.

This procedure is iterated successively until the relative error will be lower than 10^{-5} for velocity and temperature fields, and 10^{-7} for enthalpy and pressure field to achieve convergence.

$$\bar{R} = \frac{\sum |a_e \phi_e + a_w \phi_w + a_n \phi_n + a_s \phi_s + b - a_p \phi_p|}{\sum |a_p \phi_p|} \leq 10^{-7} \quad (66)$$

3.6 Code's validity

To authenticate the present numerical solution, a comparison had been done with Lu and Zhao [4], which got for the case of a uniformly heated horizontal metal-foam tube of 26 mm diameter which saturated with refrigerant R134a as the two-phase working fluid. *Figure 2* shows acceptable matching with the same case that solved by the present code with maximum error about 6%. Also, a comparison was made with experiments data of Nosrati et al. [31], which obtained for flowing R134a through a uniformly heated horizontal metal-foam annular tube. *Figure 3* shows acceptable matching with maximum error about 3%.

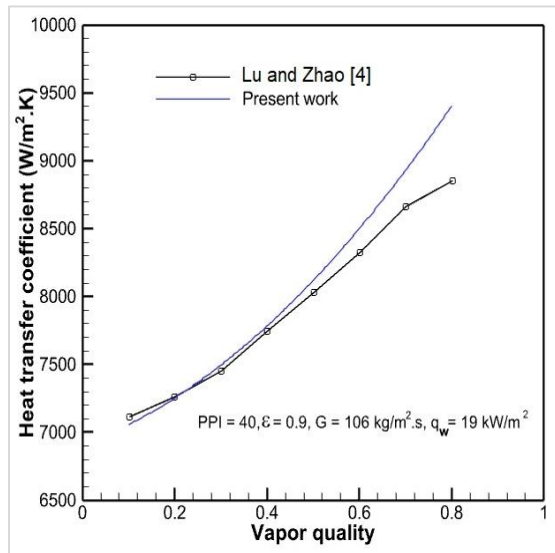


Figure 2 Comparison of the heat transfer coefficient with vapor quality between the present work and Lu and Zhao [4]

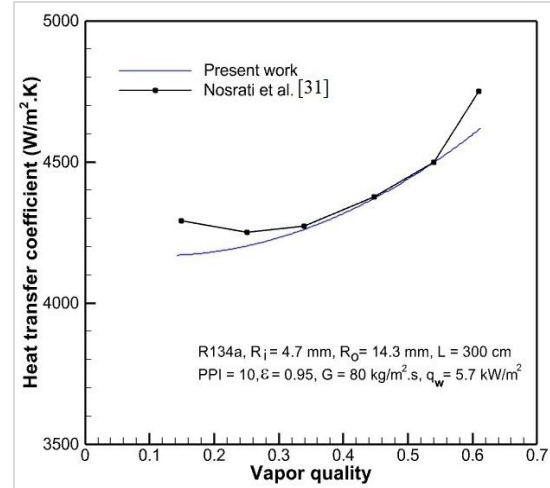


Figure 3 Comparison of the heat transfer coefficient with vapor quality between the present work and experimental data of Nosrati et al. [31]

4. Results

This study solved the problem of boiling heat transfer through an annulus of DPHEX based on LTNE model. Numerical results were accomplished for a 2 m length with 2.5 cm and 7.5 cm inner and outer diameter, which filled with copper foam of different PPI (10, 30 and 50) and ε (0.85, 0.9 and 0.95) with R134a as the working fluid. A grid independency was achieved, and the values of heat transfer coefficient appeared that the mesh of (1101×101) products a grid-independent results. All numerical results were achieved with a fixed inlet temperature $T_{in} = 18^\circ\text{C}$. The value of mass flux is selected to accomplishes ($5.01 < Re_p < 25.1$) and it is suitable to solve with the assumed model in this article [41].

Based on LTNE model, h_L can be computed as:

$$h_L = \frac{q_w}{T_{w,avg} - T_b} \quad (67)$$

where T_b is the bulk temperature of the fluid and $T_{w,avg}$ is the mean temperature at the wall of inner pipe:

$$T_{w,avg} = \varepsilon T_{wf} + (1 - \varepsilon) T_{ws} \quad (68)$$

$$T_b = \frac{\int_0^L |u| T_f dy}{\int_0^L |u| dy} \quad (69)$$

The mean heat transfer coefficient is defined as follows:

$$h_m = \frac{1}{L} \int_0^L h dx \quad (70)$$

4.1 Influence of PPI variation

The influence of the cell sizes (PPI) of the metal foam on the temperature distribution, liquid

saturation and heat transfer coefficient is presented in *Figures 4 to 7* for the case of $G = 3.5 \text{ kg/m}^2\cdot\text{s}$, $\epsilon = 0.9$. The temperature distribution of solid and fluid phases is shown as contours in *Figure 4*. At the interface wall between two pipes, the absorbed energy by metal foam (q_s) and R134a (q_f) increased with PPI increased, and as a result the temperature of solid phase raised with PPI increase that because the increase the contact points between the wall and the metal foam ligaments. As the pores density raised from 10 to 50 and with the propagation of the two-phase area, the metal foam temperature increased while the fluid phase temperature fixed at saturation temperature and the vapor region extended because of increase the convective surface area with PPI increase. When the cell size increases, the drag force produced by metal foam increases too. This may be referred to the fact that the pipe filled by metal foam with a higher cell size has a lower permeability, which causes to drop in the induced mass flux. This can explain the higher fluid temperatures for smaller cell sizes as shown in *Figure 4*.

Consequently, the presence of metal foam accelerates the evaporation process in tube. This early boiling is illustrated clearly by the liquid saturation value along the interface wall, *Figure 5*. At high PPI, it is shown that the liquid phase starts to change to vapor phase at ($x = 0.6 \text{ m}$) and liquid saturation reaches approximately to 0.8 at the pipe exit. While at low PPI, liquid starts to evaporate at ($x = 1.25 \text{ m}$) and liquid saturation reaches to 0.4. That mean, the increase in pore density increases the heat transfer between the warm and cold pipes because of the metal foam increases the active surface area of heat transfer also increases the mixing process between

the hot and cold streams and at the same time this metal foam decelerates the flow of fluid which gives more time for heat exchanging to take off.

The utilizing of LTNE model appears there is a difference between R134a and metal foam. Solid-fluid temperature difference is generally addressed as a major parameter to determine the effect of LTNE model, as seen in *Figure 6*. The raising of pore density led to decrease solid-fluid temperature difference (ΔT_{sf}) at single phase flow region, which is qualified to that the rise in pores density may increase the surface area density. But this difference will be increased with crowing in two phase flow region because of the evaporation process occurs at constant saturation temperature will metal foam still to absorb heat energy from the wall. This difference increases with increase with PPI because of increasing the contact points between the metal foam ligaments and the wall.

The local heat transfer coefficient drops gradually with horizontal direction then when evaporation process begins, it increases suddenly up to the channel exit. From *Figure 7*, the higher heat transfer coefficient is at higher PPI. This may be ascribed to increase the contact area between the metal foam and fluid which it led to creation more boiling sites. Also, the increase in the number of this smaller pores near to the interface wall will improve the flow mixing and bubbles dismantle in the evaporation region. The mean heat transfer coefficient h_m increases with pores density increase as listed in *Figure 7* for PPI = 10, 30 and 50 whereas it enhances by 96% for 50 PPI compared with 10 PPI.

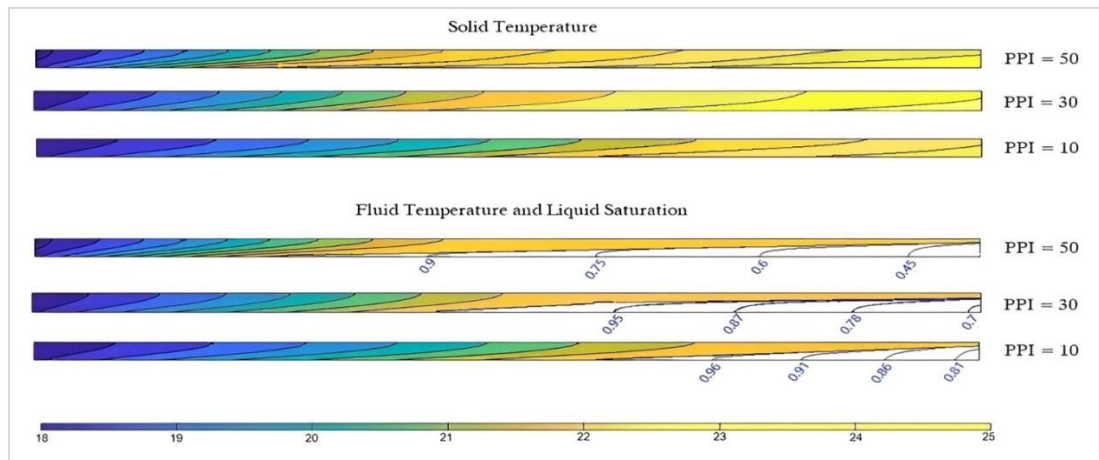


Figure 4 Influence of PPI variation at $G = 3.5 \text{ kg/m}^2\cdot\text{s}$ and $\epsilon = 0.9$

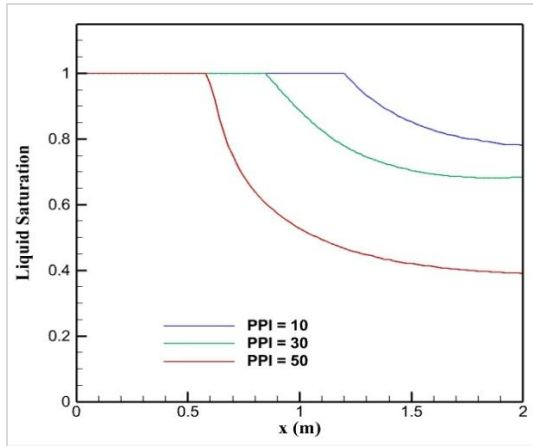


Figure 5 Liquid saturation distribution along the annulus for different PPI at $G = 3.5 \text{ kg/m}^2.\text{s}$ and $\epsilon = 0.9$

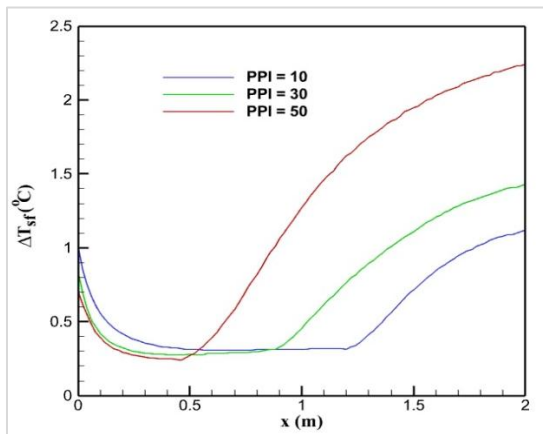


Figure 6 Temperature difference along the annulus for different PPI at $G = 3.5 \text{ kg/m}^2.\text{s}$ and $\epsilon = 0.9$

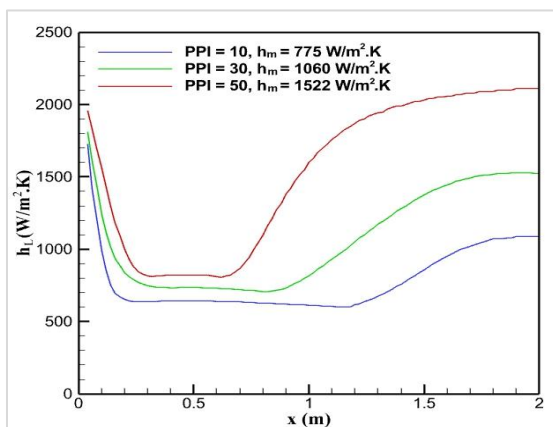


Figure 7 Variation of heat transfer coefficient along the annulus for different PPI at $G = 3.5 \text{ kg/m}^2.\text{s}$ and $\epsilon = 0.9$

4.2 Influence of mass flux variation

The effect of mass flux on the temperature distribution, liquid saturation and heat transfer coefficient is presented in *Figures 8-11* for the case of $\text{PPI} = 30$ and $\epsilon = 0.9$. When the mass flux raises, the two-phase region contracts and isotherm lines heading towards annulus outlet, as illustrated in *Figure 8*. At the same time, the buoyancy effects decrease with increasing in the inlet velocity and additional sub-cooled R134a forces the evaporation region to withdrawal towards the interface wall and it contracts as the leading edge of the sub-cooled R134a flows towards the annulus exit. Whereas the metal foam and R134a temperatures decrease with increasing in mass flux and a clear augmentation in the thermal non-equilibrium condition will be observed. As illustrated in *Figure 9*, the liquid saturation throughout the porous annulus increases with increasing in the mass flux and the vapor ratio at the exit will decrease.

Figure 10, as mass flux increases LTNE effect increased because of decreasing in residence time of the fluid in the annular pipe. Though, solid-fluid temperature difference with LTNE model augments as mass flux augments. Also, the diffusion coefficient for the temperature of R134a decreases with mass flux augmentation, which it may further cause to increase the wall heat flux. *Figure 11* illustrates the local heat transfer coefficient along the axial direction for $\text{PPI} = 30$ and $\epsilon = 0.9$. For low inlet velocity, $G = 1 \text{ kg/m}^2.\text{s}$, the evaporation point is been nearest to the annulus inlet and the local heat transfer coefficient reduces with moving from the entrance then it raises gradually until its maximum value at exit with mean value of $h_m = 740 \text{ W/m}^2.\text{K}$ as listed in *Figure 11*.

When the mass flux increases from $G = 1 \text{ kg/m}^2.\text{s}$ to $G = 3.5 \text{ kg/m}^2.\text{s}$, the inlet velocity increases which that causes contracting in the thermal boundary layer and augmentation in heat transfer coefficient especially at annulus inlet. In the contrary, the heat transfer coefficient in the evaporation area reduces when mass flux increases from $G = 3.5 \text{ kg/m}^2.\text{s}$ to $G = 6 \text{ kg/m}^2.\text{s}$ due to the reduction in mixing effect near to the interface wall which escorts the retreat in the evaporation area towards the annulus exit that linked with higher vapor ratio. Finally, the mean heat transfer coefficient reduces to $h_m = 530 \text{ W/m}^2.\text{K}$ as listed in *Figure 11*.

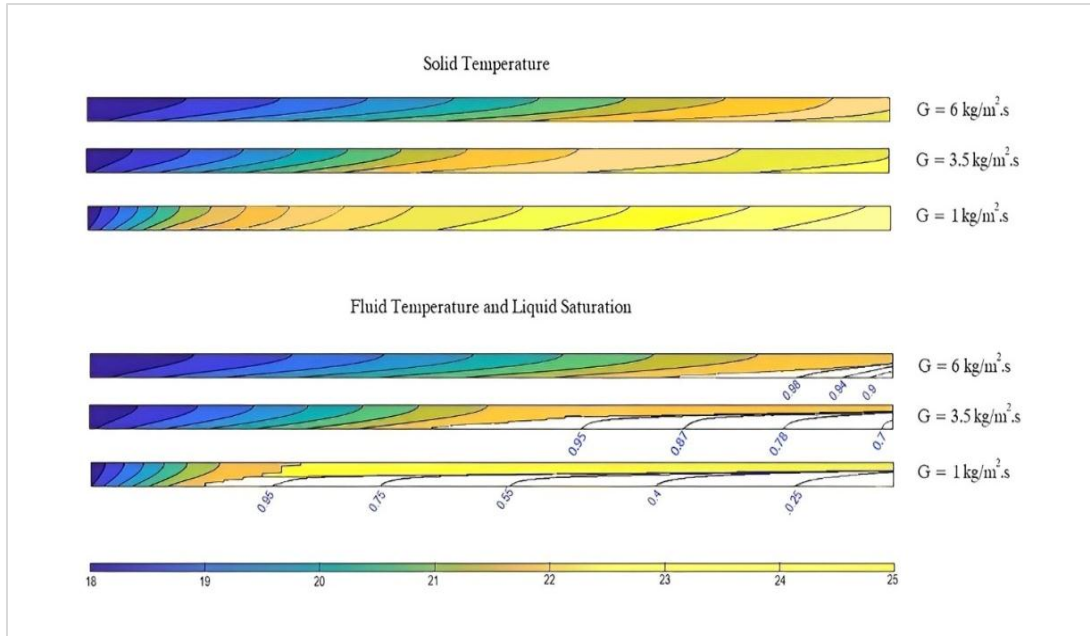


Figure 8 Influence of PPI variation at $G = 3.5 \text{ kg/m}^2 \cdot \text{s}$ and $\epsilon = 0.9$

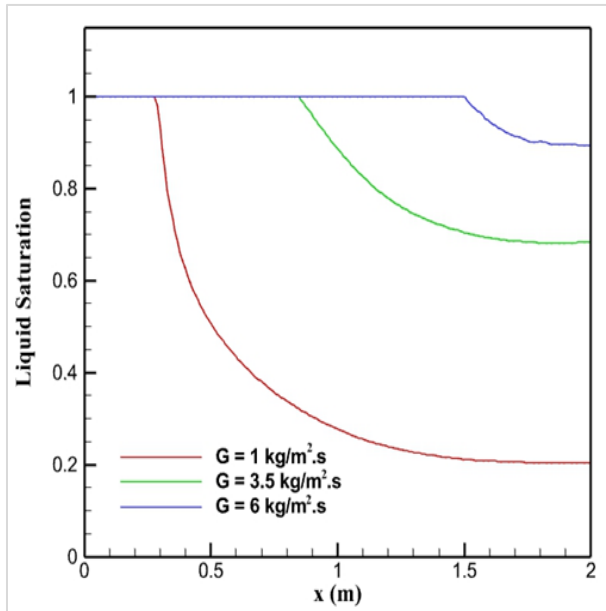


Figure 9 Liquid saturation distribution along the annulus for different PPI at $G = 3.5 \text{ kg/m}^2 \cdot \text{s}$ and $\epsilon = 0.9$

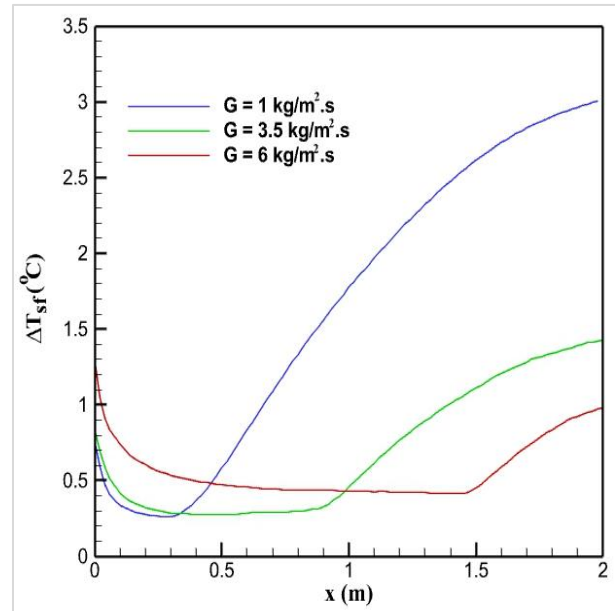


Figure 10 Temperature difference along the annulus for different PPI at $G = 3.5 \text{ kg/m}^2 \cdot \text{s}$ and $\epsilon = 0.9$

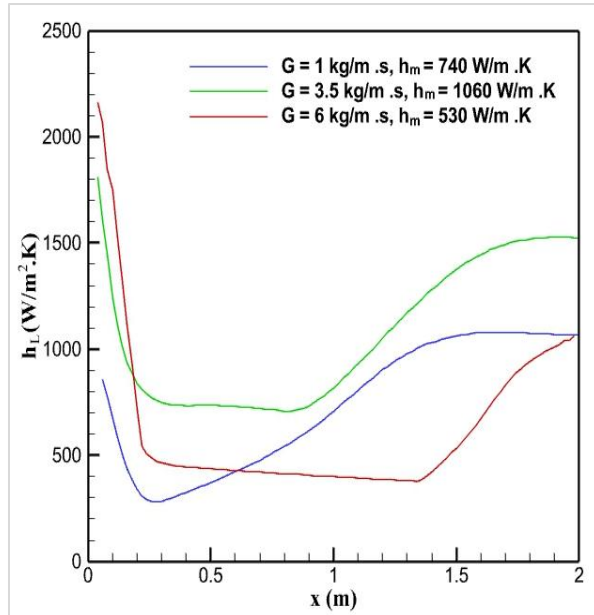


Figure 11 Local heat transfer coefficient along the annulus for different PPI at $G = 3.5 \text{ kg/m}^2.\text{s}$ and $\epsilon = 0.9$

4.3 Influence of porosity variation

The effect of metal foam porosity on the solid-fluid temperatures, liquid saturation and heat transfer coefficient is presented in *Figures 12-15* for $G = 3.5 \text{ kg/m}^2.\text{s}$ and PPI = 30. It is clear from *Figure 12* that with porosity increase, the evaporation area contracts

and the tendency of the isotherm lines heading towards the exit of annulus. *Figure 13* also appears that the liquid saturation reduces with the reduction in metal foam porosity because of decreasing in the volumetric surface area between the metal foam and R134a.

Figure 12 illustrates the effect of porosity variation on the metal foam temperature contours. With porosity increase, the temperature decreases with a clear decrease in LTNE condition with R134a.

Figure 14 indicates that solid-fluid temperature difference is less as the porosity of metal foam grows.

The local convective thermal resistance continuously increases with porosity increasing, while the conductive resistance of metal foam has slight effect on heat transfer. And for small porosity, this influence will be larger and larger on solid temperature. Therefore, the solid-fluid temperature difference initially raises and then reduces with the rise in porosity, as illustrated in *Figure 14*. *Figure 15* introduces the variation of heat transfer coefficient along the annular pipe for PPI = 30 and $G = 3.5 \text{ kg/m}^2.\text{s}$, The overall heat transfer improves by reducing the porosity of the metal foam as expected in *Figure 15*.

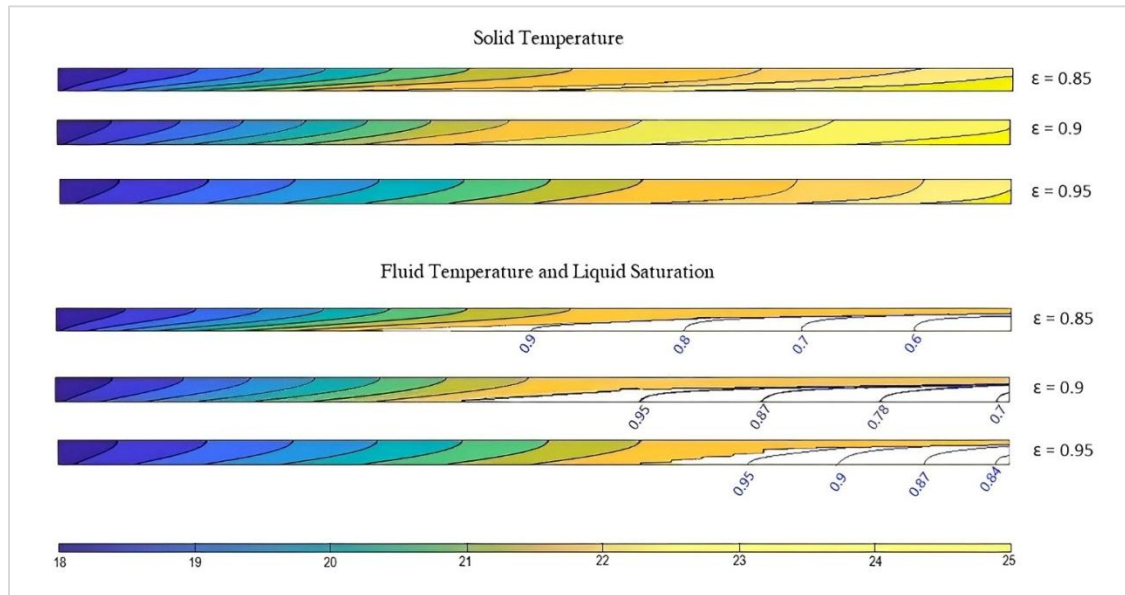


Figure 12 Influence of PPI variation at $G = 3.5 \text{ kg/m}^2.\text{s}$ and $\epsilon = 0.9$

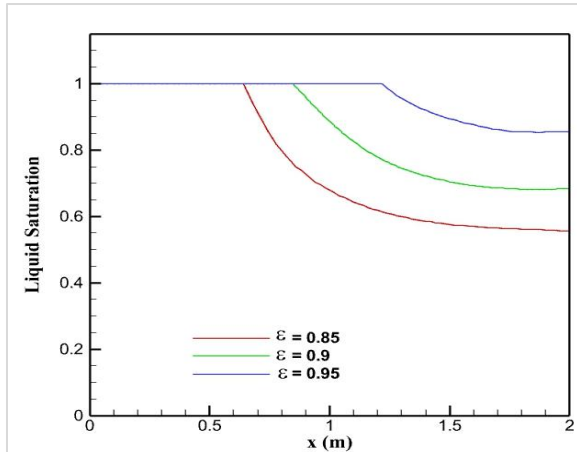


Figure 13 Liquid saturation distribution along the annulus for different PPI at $G = 3.5 \text{ kg/m}^2 \cdot \text{s}$ and $\epsilon = 0.9$

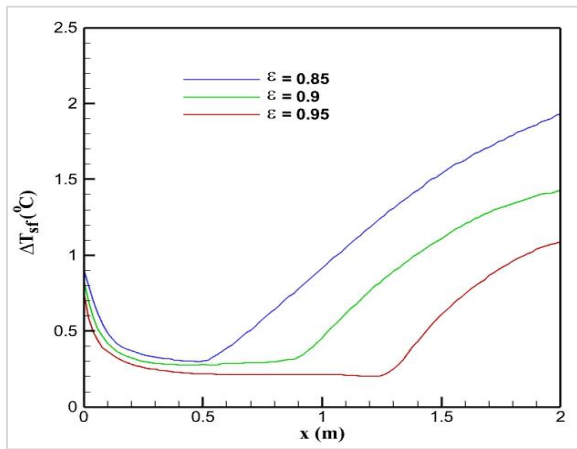


Figure 14 Temperature difference along the annulus for different PPI at $G = 3.5 \text{ kg/m}^2 \cdot \text{s}$ and $\epsilon = 0.9$

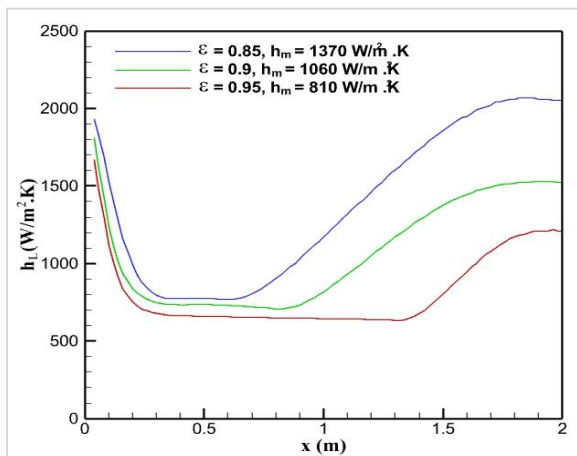


Figure 15 Variation of heat transfer coefficient along the annulus for different PPI at $G = 3.5 \text{ kg/m}^2 \cdot \text{s}$ and $\epsilon = 0$

5. Discussion

The impact of R134a evaporation parameters, such as PPI, mass flux, and porosity, on the liquid saturation and heat transfer coefficient can be assessed through MATLAB code which is built to solve and simulate the evaporation process of R134a in DPHEX. Each one of these parameters has a different effect on the evaporation process. The presence of metal foam led to increase the surface area and contact points also it works as a resistance against the flow which gives more time to heat transfer between warm parts and cold fluid and this resistance increases with porosity decrease. Whereas mass flux increasing led to increase the momentum of the flow and this increase in mass flux needs to more heat for transfer to vapor phase. The results appears that PPI has the highest effect on heat transfer coefficient and this clear when the mean heat transfer coefficient approximately doubled when PPI increased from 10 to 50 and it increased by 70% when porosity decreased from 0.95 to 0.85. The temperature difference between solid and fluid phases represents LTNE effect on evaporation process and it increases more with high PPI and low mass flux.

5.1 Limitations

It is important to verify the numerical results by conducting practical experiments. However, experimental studying the LTNE effect is more complex than that of numerical study. The measurements in metal foam are more challenging mainly due to its microstructure. The temperature measurement is difficult, in addition, the difficulty of obtaining perfect contact between the metallic foam and the hot surface as imposed in the numerical solution. Therefore, most researchers turn to the numerical solution to study the effect LTNE model on the hydrothermal properties of evaporation process through a metal foam.

A complete list of abbreviations is shown in *Appendix I*.

6. Conclusion and future work

A numerical result is achieved for evaporation heat transfer in a horizontal annulus filled with copper foam. This achievement is done by using TPMM with LTNE model. The effect of PPI, mass flux and porosity are investigated by analysing the solid-fluid temperature contours with liquid saturation values and local heat transfer coefficient. Results show that the ratio of liquid will arrive its lowest value at the outlet, and the dry out region will be shown once near the interface wall. Although LTNE effect in metal

foam is important for lower porosity, lower pore density and higher mass flux. Heat transfer coefficient reduces in the area of one phase and then increases through the evaporation area due to the increasing in mixing effect. The metal foam with small pores size (PPI) produces higher heat transfer coefficients as a result of the larger contact area. The mean heat transfer coefficient approximately doubled when PPI increased from 10 to 50 and it increased by 70% when porosity decreased from 0.95 to 0.85.

Future research can be investigated to study the effect of other parameters on the heat transfer coefficient through evaporation process with metal foam such as metal foam permeability, inlet pressure and temperature, and working fluids. Also, many different configurations of the metal foam can be studied. In addition, experimental tests are very important to know the best model to simulate this process.

Acknowledgment

None.

Conflicts of interest

The authors have no conflicts of interest to declare.

Author's contribution statement

Mohammed A. Nima: Conceptualization, writing, review and supervision. **Raed G. Saihood:** Conceptualization, writing original draft, analysis and interpretation of results.

References

- [1] He F, Dong W, Wang J. Modeling and numerical investigation of transient two-phase flow with liquid phase change in porous media. *Nanomaterials*. 2021; 11(1):1-14.
- [2] Wang CY. A fixed-grid numerical algorithm for two-phase flow and heat transfer in porous media. *Numerical Heat Transfer*. 1997; 32(1):85-105.
- [3] Wang JH, Wang HN. A discussion of transpiration cooling problems through an analytical solution of local thermal nonequilibrium model. *Journal of Heat and Mass Transfer*. 2006; 128(10):1093-8.
- [4] Lu W, Zhao CY. Numerical modelling of flow boiling heat transfer in horizontal metal-foam tubes. *Advanced Engineering Materials*. 2009; 11(10):832-6.
- [5] Alomar OR, Mendes MA, Trimis D, Ray S. Simulation of complete liquid-vapor phase change inside divergent porous evaporator. *International Journal of Materials, Mechanics and Manufacturing*. 2014; 2(3):223-9.
- [6] Xu HJ, Gong L, Zhao CY, Yang YH, Xu ZG. Analytical considerations of local thermal non-equilibrium conditions for thermal transport in metal foams. *International Journal of Thermal Sciences*. 2015; 95:73-87.
- [7] Alomar OR. Numerical investigation of two-phase flow in a horizontal porous evaporator with localised heating using non-Darcian flow and two equations model. *Heat and Mass Transfer*. 2020; 56(4):1203-21.
- [8] Alomar OR. Transient behaviour of heat transfer with complete evaporation process in porous channel with localised heating using non-darcian flow and LTNE model. *Heat and Mass Transfer*. 2021; 57(12):1921-48.
- [9] Liu T, Su H, Chen Z, He F, Wang J. Numerical investigation on the transient transport and heat transfer characteristics of transpiration cooling with liquid phase change during coolant adjustment. *Applied Thermal Engineering*. 2022.
- [10] Abdulmajeed BA, Jawad HR. CFD application on shell and double concentric tube heat exchanger. *Journal of Engineering*. 2019; 25(2):136-50.
- [11] Chen X, Tavakkoli F, Vafai K. Analysis and characterization of metal foam-filled double-pipe heat exchangers. *Numerical Heat Transfer, Part A: Applications*. 2015; 68(10):1031-49.
- [12] Hamzah JA, Nima MA. Numerical investigation of heat transfer enhancement of double pipe heat exchanger using metal foam fins. *Journal of Engineering*. 2019; 25(6):1-18.
- [13] Mohammadi MH, Abbasi HR, Yavarinasab A, Pourrahmani H. Thermal optimization of shell and tube heat exchanger using porous baffles. *Applied Thermal Engineering*. 2020; 170:1-17.
- [14] Nima MA, Hajeej AH. Experimental investigation of convection heat transfer enhancement in horizontal channel provided with metal foam blocks. *Journal of Engineering*. 2016; 22(5):144-61.
- [15] Saleh AA, Rashid TA. Experimental and theoretical study for performance enhancement of air solar collectors by using different absorbers. *Al-Khwarizmi Engineering Journal*. 2016; 12(3):110-20.
- [16] Arjun J, Annamalai M. Optimization of Foam Characteristics for Falling Film Evaporators. *International refrigeration and air conditioning conference*. 2018(pp.1-9).
- [17] Stepanov O, Rydalina N, Antonova E. The use of porous metals in heat exchangers. In *IOP conference series: materials science and engineering 2020* (p. 012150). IOP Publishing.
- [18] Dehghan M, Jamal-Abad MT, Rashidi S. Analytical interpretation of the local thermal non-equilibrium condition of porous media imbedded in tube heat exchangers. *Energy Conversion and Management*. 2014; 85:264-71.
- [19] Xu HJ, Qu ZG, Tao WQ. Numerical investigation on self-coupling heat transfer in a counter-flow double-pipe heat exchanger filled with metallic foams. *Applied Thermal Engineering*. 2014; 66(1-2):43-54.
- [20] Trilok G, Kumar KK, Gnanasekaran N, Mobedi M. Numerical assessment of thermal characteristics of metal foams of orderly varied pore density and porosity under different convection regimes. *International Journal of Thermal Sciences*. 2022.

- [21] Paknahad R, Siavashi M, Hosseini M. Pore-scale fluid flow and conjugate heat transfer study in high porosity Voronoi metal foams using multi-relaxation-time regularized lattice Boltzmann (MRT-RLB) method. *International Communications in Heat and Mass Transfer*. 2023.
- [22] Diganjit R, Gnanasekaran N, Mobedi M. Numerical study for enhancement of heat transfer using discrete metal foam with varying thickness and porosity in solar air heater by LTNE method. *Energies*. 2022; 15(23).
- [23] Tamkhade PK, Lande RD, Gurav RB, Lele MM. Investigations on tube in tube metal foam heat exchanger. *Materials Today: Proceedings*. 2023; 72:951-7.
- [24] Iranmanesh A, A. Moshizi S. Flow and heat transfer study of an annulus partially filled with metallic foam on two wall surfaces subject to asymmetrical heat fluxes. *Arabian Journal for Science and Engineering*. 2023:1-8.
- [25] Maiorano LP, Castillo R, Molina JM. Al/Gf composite foams with SiC-engineered interfaces for the next generation of active heat dissipation materials. *Composites Part A: Applied Science and Manufacturing*. 2023.
- [26] Ginting FH, Tetuko AP, Asri NS, Nurdiyansah LF, Setiadi EA, Humaidi S, et al. Surface treatment on metal foam wick of a ferrofluid heat pipe. *Surfaces and Interfaces*. 2023:1-11.
- [27] George GR, Bockelmann M, Schmalhorst L, Beton D, Gerstle A, Lindermeir A, et al. Optimization of metal foam pellet shape in packed beds for improved radial heat transfer using particle-resolved computational fluid dynamics. *Chemical Engineering and Processing-Process Intensification*. 2023.
- [28] Gao W, Xu X, Liang X. Flow boiling of R134a in an open-cell metal foam mini-channel evaporator. *International Journal of Heat and Mass Transfer*. 2018; 126:103-15.
- [29] Nam S, Kim DY, Kim Y, Kim KC. Effect of metal foam insert configurations on flow boiling heat transfer and pressure drop in a rectangular Channel. *Materials*. 2021; 14(16).
- [30] Li L, Yao H, Wang Y, Chen H, Zhu Y. Performance characteristics of the metal foam wick prepared by magnetron sputtering method. *Journal of Thermophysics and Heat Transfer*. 2021; 35(4):669-76.
- [31] Nosrati A, Akhavan-Behabadi M, Sajadi B, Razi P, Mohammadi R. Experimental study on the effects of using metal foam on R-134a flow boiling in annular tubes. *International Journal of Thermal Sciences*. 2022.
- [32] Kisitu D, Caceres C, Zlatinov M, Schaffarzick D, Ortega A. Experimental investigation of r134a flow boiling in copper foam evaporators for high heat flux electronics cooling. In *international electronic packaging technical conference and exhibition 2022* (p. V001T08A003). American Society of Mechanical Engineers.
- [33] Kang Y, Lang Z, Wu G, Zhao H. Synergistic effect of coating copper foam with carbon nanotubes on pool boiling heat transfer performance. *Experimental Thermal and Fluid Science*. 2023.
- [34] Li H, Fan Z, Lai Q, Xie Y, Qiao L, Tan J. The effect of pulse heating on saturated boiling heat transfer in rough surfaces. *Case Studies in Thermal Engineering*. 2023.
- [35] Yue SJ, Xu ZG. Numerical simulation on pore-scale pool boiling mechanisms of horizontal gradient porous metals. *International Communications in Heat and Mass Transfer*. 2023.
- [36] Wang H, Ying QF, Lichtfouse E, Huang CG. Boiling heat transfer in copper foam bilayers in positive and inverse gradients of pore density. *Journal of Applied Fluid Mechanics*. 2023; 16(5):973-82.
- [37] Nima M. Numerical study of phase change characteristics in a vertical and inclined porous channel using thermal nonequilibrium model. *Journal of Porous Media*. 2016; 19(12): 1099-121.
- [38] Rohsenow WM. A method of correlating heat-transfer data for surface boiling of liquids. *Transactions of the American Society of Mechanical Engineers*. 1952; 74(6):969-75.
- [39] Xiao H, Liu Z, Liu W. Conjugate heat transfer enhancement in the mini-channel heat sink by realizing the optimized flow pattern. *Applied Thermal Engineering*. 2021; 182.
- [40] Patankar S. *Numerical heat transfer and fluid flow*. Taylor & Francis; 2018.
- [41] Kaviany M. *Principles of heat transfer in porous media*. Springer Science & Business Media; 2012.



Mohammed A. Nima received the M.Sc. and Ph.D. degrees in Mechanical Engineering from University of Baghdad, Iraq, in 2008 and 2012 respectively. He is currently working as an assistant professor in the Mechanical Engineering Department, University of Baghdad, 10071 Baghdad, Iraq. His current research interests include Solar Energy, Computational Fluid Dynamic, Mixed Convection Heat Transfer with Phase Change and Heat Transfer Analysis in Porous Media.

Email: dralsafi@uobaghdad.edu.iq



Raed G. Saihood received the M.Sc. and Ph.D. degrees in Mechanical Engineering from University of Baghdad, Iraq, in 2007 and 2015 respectively. He is currently working as a Lecturer in the Mechanical Engineering Department, University of Baghdad, 10071 Baghdad, Iraq. His current research interests include porous media/flow and heat transfer, computational fluid dynamics, convection heat transfer and cooling of electronic equipment.

Email: raed.hassan@coeng.uobaghdad.edu.iq

Appendix I

S. No.	Abbreviation	Description
1	BFED	Brinkman-Forchheimer-Extended Darcy
2	CFD	Computational Fluid Dynamics
3	DPHEX	Double Pipe Heat Exchanger
4	LTE	Local Thermal Equilibrium
5	LTNE	Local Thermal Non-Equilibrium
6	PPI	Pores Per Inch
7	SFM	Separate Flow Model
8	TPMM	Two-Phase Mixture Model